Desalination and Water Treatment
www.deswater.com

doi: 10.5004/dwt.2021.27822

241 (2021) 112–123
November

Removal of fluoride using bagasse activated carbon

Neeraj Chandraker[a], Raghwendra Singh Thakur[a,*], Parmesh Kumar Chaudhari[b]

[a]*Department of Chemical Engineering, School of Studies of Engineering and Technology, Gurughasidas University Bilaspur – 495009, Chhattisgarh, India, emails: chandraker.neeraj@gmail.com (N. Chandraker), raghurpr@gmail.com (R.S. Thakur)*
[b]*Department of Chemical Engineering, National Institute of Technology Raipur, Raipur – 492001, India, email: pkchaudhari.che@nitrr.ac.in*

Received 22 October 2020; Accepted 7 September 2021

ABSTRACT

Bagasse activated carbon (BAC) was prepared from sugarcane bagasse to remove fluoride from a high concentration, 10–50 mg/L, synthetic fluoride-containing water. The role of pH, temperature, adsorbent dose, initial concentration and contact time in defluoridation were assessed. Results showed that BAC reduced the fluoride concentration from 50 to 9.8 mg/L at 26°C, while the concentration of 10 mg/L was reduced to 0.8 mg/L which is within the safe fluoride concentration limit of 1.5 mg/L specified by the World Health Organization (WHO). Kinetic, isotherm and thermodynamic studies were performed to analyze the nature of the fluoride adsorption process over BAC.

Keywords: Fluoride removal; Sugarcane bagasse; Activated carbon; Adsorption

1. Introduction

While fluoride (F^-) in small concentration (0.5–1.5 mg/L) is beneficial for human health, its concentration above the safe limit (1.5 mg/L) in drinking water as authorized by the World Health Organization (WHO), may cause damage to kidney, liver, demineralize bones and tooth tissue leading to dental fluorosis. Fluorine is highly reactive and therefore it is usually found in a combined state [1]. The presence of F^- in the groundwater may be due to the contribution of several factors, such as natural occurrence, rock weathering, deposition by effluents from industries or by geochemical reactions [2–4]. Fluoride concentration in India varies from 4.21 mg/L in Kashmir to 48 mg/L in Haryana and more than 19 of its states have high F^- concentration in their groundwater [5]. On the other hand, Yadav et al. [6] compiled the F^- concentration in various states of India, as reported by various researchers, which shows its variation from 2 mg/L in Haryana to 38 mg/L in Rajasthan. This may be due to the reason that water quality varies from place to place even in the same state. However, those data indicate that the concentration of fluoride in several places of India is at an alarming level and is detrimental to the natives of those places. Further, the allowable F^- concentration in the effluent from a wastewater plant is 4 mg/L as set by the United States Environmental Protection Agency (USEPA) and [1]. Hence, the removal the fluoride through a cheap and effective method is a mandate to avoid the deleterious effect on health.

Common defluoridation techniques include, precipitation with alum and lime, activated alumina, adsorption, ion exchange process, electrodialysis, reverse osmosis [7,8], microwave catalysis [9,10] and photocatalysis [11,12]. While membrane and electrodialysis are effective techniques to reduce the fluoride concentration within permissible limits, they are expensive as well as they suffer from operational difficulties such as frequent cleaning of the membrane [13]. Preparation and regeneration of catalyst impede the uses of photocatalysis and microwave catalysis process.

* Corresponding author.

Adsorption, on the other hand, is a favorable technique due to the variety of adsorbents available and the flexibility of operation. In F^- removal through adsorption, finding a suitable low-cost adsorbent with high uptake capacity and easy regeneration has been a focus of research. In this regard, biosorbents have been an attractive choice [14]. Rice husk (fluoride concentration 5–23 mg/L) and activated rice husk (1.5–15 mg/L), chemically activated groundnut (1–10 mg/L), coconut (10 mg/L), walnut shells (1–10 mg/L), peels of substances like a banana (6.72 mg/L), pineapple (1–4 mg/L) and lemon (20 mg/L), the terms in the bracket denoting fluoride concentration in the solution, are some of the biosorbents that have shown fluoride adsorption capacity in the range 0.4–15 mg/g [15]. Bael (*Aegle marmelos*) shell-activated carbon has shown a fluoride adsorption capacity of 2.45 mg/g (8 mg/L) [16]. Araga et al. [17] used KOH treated Jamun seed (*Syzygium cumini*) and observed fluoride removal capacity to be 3.65 mg/g of adsorbent. Activated bagasse carbon was reported to give 1.16 mg/g of fluoride adsorption capacity from a solution containing 5 mg/L of fluoride [18]. Another study on fluoride removal using sugarcane bagasse reports adsorption capacity to be 4.12 mg/g for fluoride concentration of 8 mg/L [19].

One of the important criteria for the selection of biosorbent is its low cost and availability in addition to its adsorption capacity [14]. Sugarcane bagasse (*Saccharum officinarum*) is a fibrous waste generated in large amount during the extraction of sugarcane and in this process, one ton of sugarcane gives about 280 kg of bagasse [20]. According to the Global Agriculture Information Network (GAIN) Report (number IN8047) the sugarcane production in India for the year 2018–19 was about 400 million metric tonnes [21]. Though the sugarcane bagasse is used as a fuel to support sugar enterprises, its large amount remains unutilized [22]. Since the fluoride concentration in groundwater in some parts of India is as high as 38 mg/L and also considering that the sugarcane bagasse is abundantly available, in this work bagasse was chosen as a precursor to prepare activated carbon adsorbent to remove fluoride from synthetic water having fluoride concentration 50 mg/L as a base case. The effect of various parameters such as pH, contact time and adsorbent dose, temperature and initial fluoride concentration were examined to find the optimum parameters for defluoridation of the solution.

2. Materials and methods

2.1. Preparation of H_3PO_4 treated bagasse activated carbon

Sugarcane bagasse waste was acquired from the local market of Raipur Chhattisgarh. Bagasse was washed with tap water then with distilled water to remove dust particles in the material. It was then dried for 24 h in a hot-air oven at 120°C; crushed and sieved to get even grain size; carbonized by heating for 2 h at 500°C without adding any chemical agent. The carbon so produced was treated with 30% phosphoric acid in an equal weight ratio for 24 h followed by washing with distilled water and then drying. This activated carbon obtained was named bagasse activated carbon (BAC) and it was stored in vacuum desiccators for further study.

2.2. Characterization of BAC

The surface morphology and the elemental analysis of the BAC were done in a ZEISS EVO Series scanning electron microscope (SEM) model which also contained an energy-dispersive analysis of the X-ray (EDX) feature. The Brunauer–Emmett–Teller (BET) surface area of BAC was determined by using nitrogen adsorption isotherms methods at 77 K by surface area analyzer (Model – SMART SORB 93) surface. The point of zero charges was determined by the solid addition method [19].

2.3. Batch adsorption experiment

Lab-scale studies to remove F^- from synthetic fluoride bearing water were carried out. To prepare the stock solution of concentration 50 mg/L, 110.5 mg of anhydrous sodium fluoride was dissolved in 1 L of distilled water. Batch adsorptive treatment of F^- bearing water was carried out in a shaker taking 50 mL of sodium F^- solution contaminating 50 mg/L F^- in a 100 mL conical flask. About 5 mL samples were taken at a certain time interval and F^- the content was determined. Effect of pH, adsorbent dose (g) and contact (shaking) time on F^- removal was estimated. The F^- removal efficiency after adsorption was estimated using Eq. (1), and uptake capacity of adsorbent at any time (t) was estimated using Eq. (2).

$$R\% = \frac{C_0 - C_t}{C_0} \times 100 \tag{1}$$

$$q_t = \frac{\left(C_0 - C_t\right)V}{m} \tag{2}$$

where $R\%$ is the percentage removal efficiency; C_0 is the initial concentration, mg/L; C_t is the concentration after time t, mg/L; V is volume of solution, L; m is mass of adsorbent, g.

3. Results and discussion

3.1. Characterization of adsorbent

The SEM images of BAC prior to adsorption are shown in Fig. 1a and after to adsorption in Fig. 1b. After adsorption, some dense mass is seen which may be due to the retention of pollutants present in water. The structure of the adsorbent is more like flakes and no obvious porous structure is detectable at that resolution. The EDX analysis before adsorption is shown in Fig. 1c and after to adsorption in Fig. 1d. The main components present are C, Si, and Ca earlier to adsorption, and after adsorption, F is also seen which is due to its retention in adsorbent in the adsorption process. The BET surface area of the BAC was found to the 812 m^2/g.

The point of zero charge (pH_{pzc}) analysis gives an idea about the surface charge over an adsorbent. It is obtained by plotting the difference of initial pH to final pH against the initial pH of the solution and the pH at which this difference becomes zero, which is noted as pH_{pzc}. When the solution pH is less than the pH_{pzc}, the adsorbent surface will be positively charged and it will attract negative ions. Whereas, when the pH of the solution is more than the pH_{pzc} the adsorbent

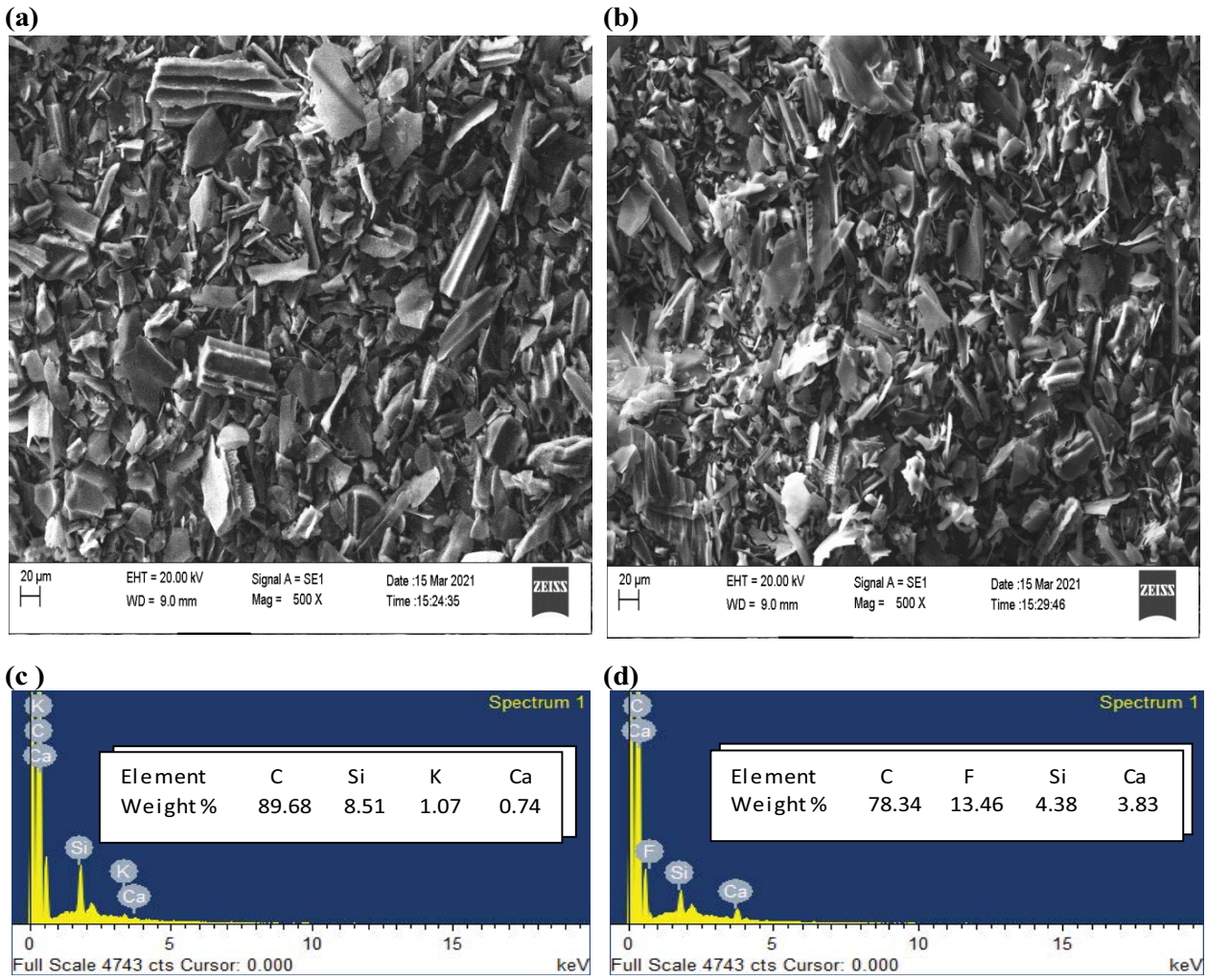

Fig. 1. SEM of BAC (a) before adsorption, (b) after adsorption; EDX of BAC (c) before adsorption, (d) after adsorption.

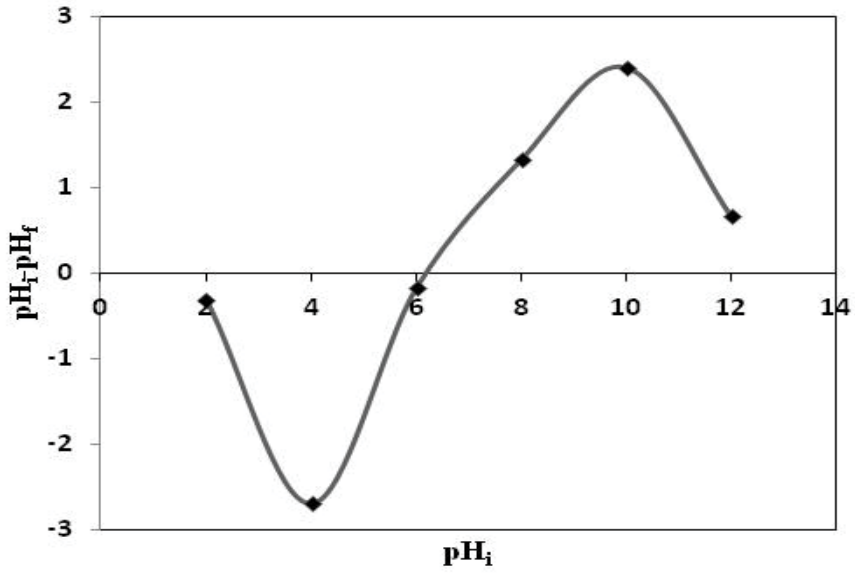

Fig. 2. pH_{pzc} for the BAC adsorbent.

surface is negatively charged and it could adsorb positive ions. From Fig. 2 the pH_{pzc} was found to be 6.1 for BAC.

Nitrogen adsorption–desorption isotherms at –196°C are presented in Fig. 3a for prepared carbon particle size of 0.225 mm and this hysteresis loop shows the presence of microporous. Due to the presence of micropores, the amount of adsorbed nitrogen increased at low relative pressure (0.1) as presented by the initial steep in Fig. 3a. In addition, the pore size distribution of the same material is presented in Fig. 3b which shows that the samples had narrow particle size distribution in ranges of 0.6–0.8 nm. The pore size distribution depends on the average particle diameter and characteristics of the material [23,24].

3.2. Effect of pH

Alteration in pH changes the surface charge of adsorbent which in turn affects the adsorption [25]. At a lower pH value the negative charges at the adsorbent surface are reduced, thus it can adsorb anions more readily than cations from solutions [26,27]. The pH dependence occurs when the F^- ions and hydroxyl ions compete for adsorption sites or when the ions and protons compete for the same active binding sites on the sorbent surface [28] Therefore, maintaining a proper pH to affect defluoridation is very important.

The effect of initial pH (pH_i) on the adsorption process was studied for the range 2–10, and the results are presented in Fig. 4. An increase in pH from 2 to 4 favored the defluoridation, but further increase in pH adversely affected the defluoridation. The optimum pH was observed as 4 where, the initial fluoride concentration (F_i) of 50 mg/L was reduced to 12 mg/L in the solution after 4 h of contact time, at an adsorbent dose of 4 g/L and the shaking speed of 100 rpm. Further studies were performed at an initial solution pH of 4 only.

3.3. Effect of adsorbent size

To investigate the effect of particle size, experiments were performed with the particle size of 0.225, 0.45 and 0.90 mm. The larger surface area provides better per unit adsorption and as anticipated better F^- removal was observed with the particle size of 0.225 mm compared to the other two particle sizes as shown in Fig. 5. The final fluoride concentration in the solution were 12.0, 18.0 and 27.4 mg/L for 0.225 mm, 0.45 mm and 0.90 mm adsorbent respectively. Therefore, the adsorbent size of 0.225 mm was chosen for further studies.

3.4. Effect of temperature and mass loading

Temperature is an important factor that greatly affects the adsorption process. An increase in temperature increases the mobility of sorbate from the solid surface to the solution phase due to a decrease in the thickness of the boundary layer. The effect of temperature on adsorptions likewise

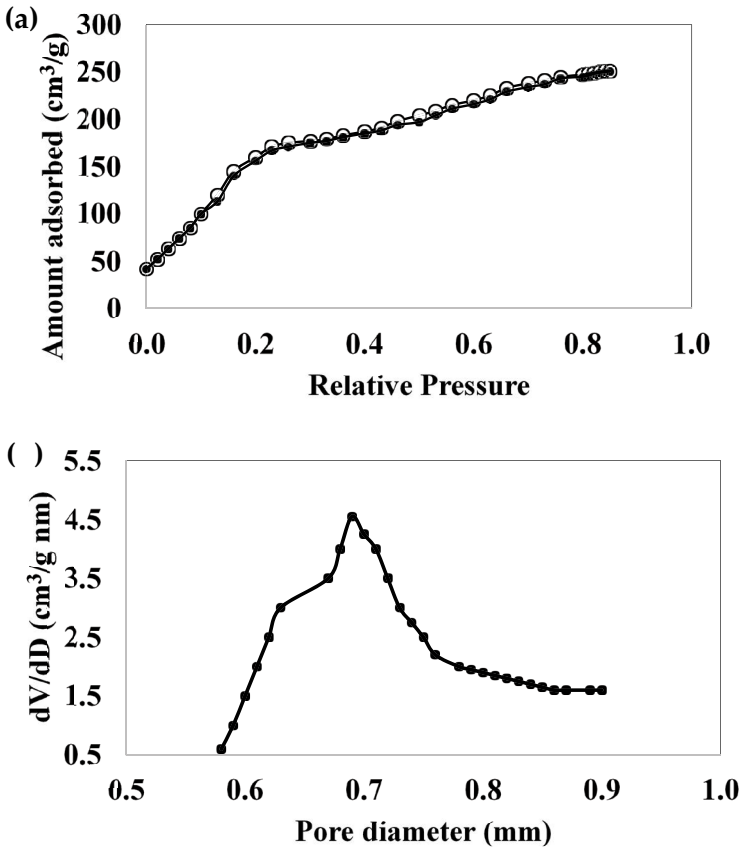

Fig. 3. (a) N_2 adsorption–desorption curves and (b) micropore size distribution of 0.225 mm size of prepared carbon.

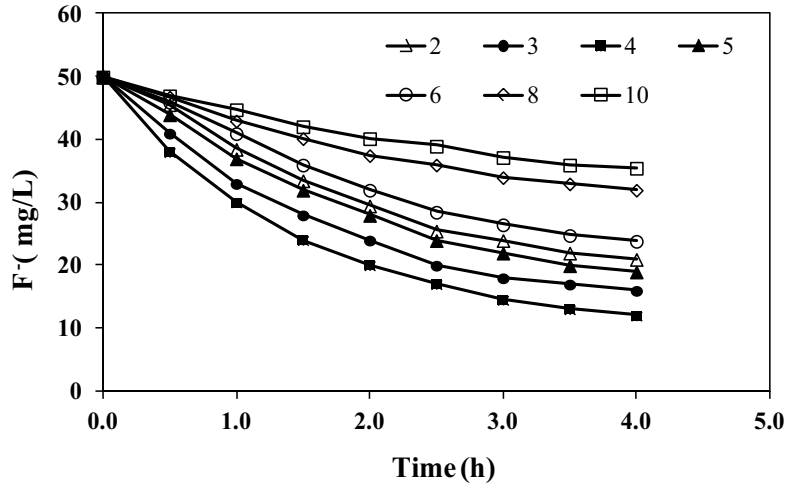

Fig. 4. Effect of pH_i on removal of F^- using BAC. Initial concentration of F^- = 50 mg/L; BAC dose = 4 g/L; adsorbent size = 0.225 mm; temperature = 26°C.

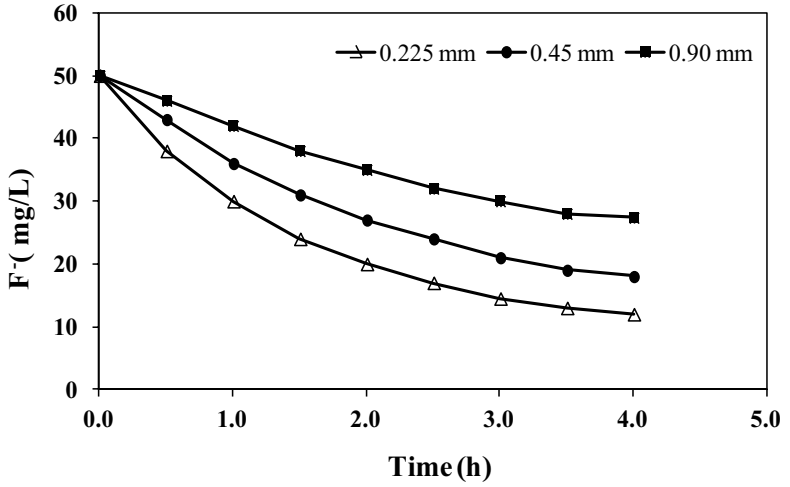

Fig. 5. Effect of BAC size on removal of F^-. Initial concentration of F^- = 50 mg/L; BAC dose = 4 g/L; pH_i = 4; temperature = 26°C.

relies upon the warmth of sorption. In general, adsorption is an exothermic process and it is favored at low temperature [29,30].

Adsorbent mass loading or adsorbent dose is the amount of adsorbent brought into contact with the solute. The adsorption efficiency of an adsorbent increases with the adsorbent dose. This is due to the availability of more adsorption sites. However, the adsorption density (amount of sorbate per unit weight of adsorbent) reduces due to unsaturated adsorption sites. Adsorption density is also reduced due to particle interactions caused by high adsorbent concentrations. The reason for the high removal of F^- with an increase in adsorbent mass is due to the availability of a larger amount of surface for adsorption at its higher dose [18].

Effect of temperature and mass loading was studied in the temperature range 16°C–46°C and mass loading 3–6 mg/L. The final concentration of F^- in the solution was 13.8, 10, 8.8, and 8.4 mg/L at 16°C; 16, 12, 9.8 and 9 mg/L at 26°C; 21.3, 17, 15 and 14 mg/L at 36°C; 29.2, 24.2, 20 and 18.8 mg/L at 46°C for adsorbent dose of 3, 4, 5, and 6 mg/L, respectively. The detailed data are presented in Fig. 6a–d. For all mass loading, the F^- removal decreased when the temperature was increased. Since there was only a marginal change in the final concentration of F^- with the increase in adsorbent dose from 5 to 6 mg/L for the temperature range studied, the former was taken as the optimum adsorbent dose.

3.5. Effect of temperature and initial concentration of F^-

The effect of the initial concentration of F^- and temperature on its removal is presented in Fig. 7a–d. For all the concentrations (10–50 mg/L) F^- removal was increased when the temperature was decreased. Higher removal of F^- was seen at its low concentration. The final F^- concentrations were, 0.7, 2.4, 4.5, 6.5, 8.8 at 16°C; 0.8, 2.5, 4.7, 6.8, 9.8 at 26°C; 1.5, 3.6 6.5, 10, 15 at 36°C and 2.8, 4.6, 7.6, 12, 20 at 46°C for 10, 20, 30, 40 and 50 mg/L of F_i respectively. But for 46°C temperature, the initial F^- concentration of 10 mg/L

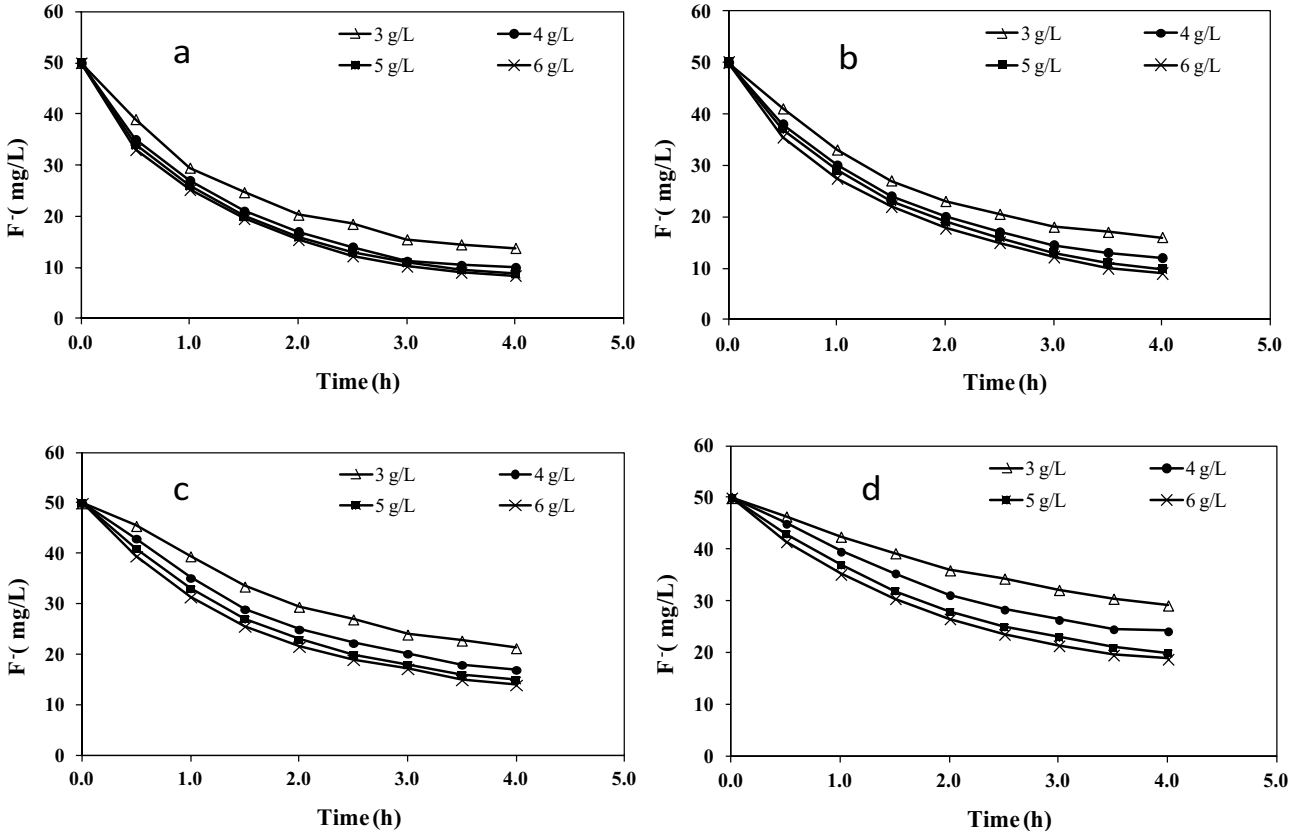

Fig. 6. Effect of BAC doze on removal of F^- for initial concentration of F^- = 50 mg/L; pH_i = 4; at temperature (a) 16°C, (b) 26°C, (c) 36°C, and (d) 46°C.

was decreased to less than or equal to the limiting value of fluoride concentration in drinking water (1.5 mg/L) for all other temperatures. It is observed that initial ion concentration significantly affects the adsorption efficiency. As concentrations of adsorbent increase, there is an expansion in the number of ions bound yet the rate of amount adsorbed diminishes. An increment in the measure of ions adsorbed with an increase in concentrations has been ascribed to the availability of binding sites present on the sorbent [31,32].

3.6. Effect of contact time

The concentration of fluoride in the solution was measured from 0 to 4 h at time intervals of 0.5 h. The study showed that the rate of decrease of fluoride concentration in the solution was initially higher followed by a lower rate. This is due to occupying vacant sites, and reduction in available surface area for adsorption with time [33,34]. After 3.5 h the rate of adsorption became very slow and the concentration of fluoride became almost constant with further increase in time. Therefore 4 h was fixed as a desirable contact time for fluoride removal.

3.7. Adsorption kinetics study

To get an insight of fluoride adsorption mechanism the kinetics studies were performed at 16, 26, 36 and 46°C, for adsorbent dose 5 mg/L and initial pH 4. The pseudo-first-order [35], pseudo-second-order [36], Elovich model [37] and pore diffusion model [38], as shown in Eqs. (3)–(6) respectively, were tested in the present adsorption process. Since, the linearization of these models may cause alteration in model parameter value, leading to erroneous interpretation of the kinetic data, their nonlinear forms were used [39–43]. To estimate the model parameter/s, the sum of the square of the errors (SSE) between the experimental q_t and the model calculated q_t [42] was minimized using the "Solver Add-In" of Microsoft Excel. The resulting value of parameter/s, at the minimized SSE, was taken as their final estimate.

Pseudo-first-order model:

$$q_t = q_e\left(1 - e^{-K_1 t}\right) \tag{3}$$

where q_e is the equilibrium uptake capacity of adsorbent (mg of fluoride/g of adsorbent). The first-order constant K_1 is indicative of the kinetic rate of the process. A larger value of K_1 suggests quicker adsorption thus less time to reach equilibrium [44,45].

Pseudo-second-order model:

$$q_t = \frac{K_2 q_e^2 t}{1 + K_2 q_e t} \tag{4}$$

where K_2 is the pseudo-second-order rate constant (g/mg h). Pseudo-second-order model is tested to ascertain

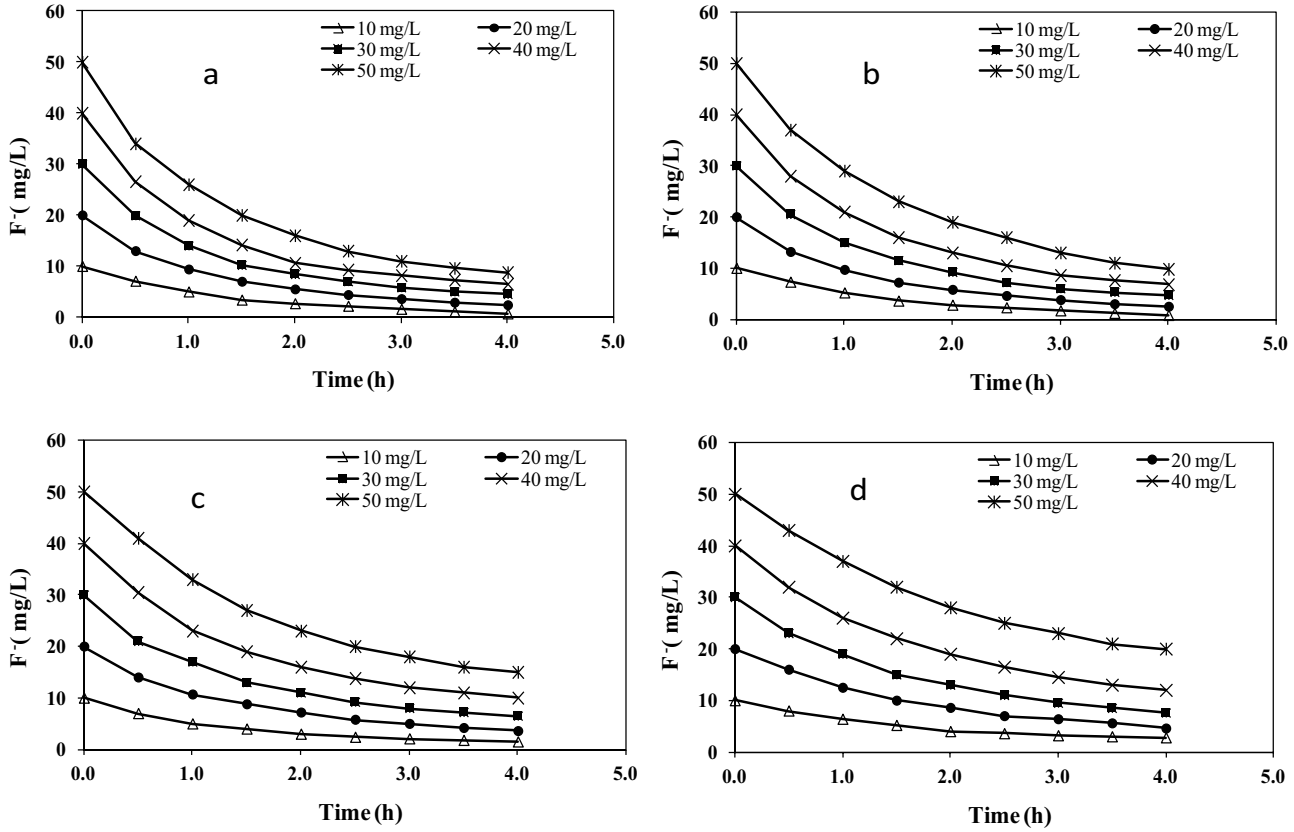

Fig. 7. Effect of initial concentration of F^- on its removal for pH_i = 4, adsorbent dose 5 g/L at temperature (a) 16°C, (b) 26°C, (c) 36°C, and (d) 46°C.

the chemisorption behavior of the adsorption process. The term $K_2q_e^2$ gives an idea about the initial sorption rate [45].

Elovich model:

$$q_t = \frac{1}{b}\ln\left(1+abt\right) \tag{5}$$

where a (initial adsorption rate) and b (desorption rate) are the Elovich constants. Constant $1/b$ is indicative of available sites for adsorption. The Elovich model neglects desorption but suitability describes kinetic data representing the chemisorption mechanism of the adsorption process [46].

Pore diffusion model:

$$q_t = K_i t^{0.5} + C \tag{6}$$

where K_i (mg/g $h^{0.5}$) is the intraparticle rate constant and C (mg/g) is the initial rate of adsorption. The fitness of the model to kinetic data validates the involvement of intra-particle diffusion in the adsorption process.

The coefficients estimated for various kinetic models are shown in Table 1. The R^2 and the SSE values presented in Table 1 for different kinetic models suggest that the pseudo-first-order and Elovich models fit well to the kinetic data. The fitness of the pseudo-first-order model indicates the involvement of the physical adsorption mechanism in the early stages of adsorption while in the later part chemisorption prevails as suggested by the Elovich model [47].

3.8. Adsorption isotherm

Adsorption isotherm models are used to describe the relationship between adsorption capacity and equilibrium concentration. Langmuir, Freundlich and Temkin isotherms are widely used for this [43]. The parameters of the isotherm models were estimated through a nonlinear regression technique, similar to that described in the adsorption kinetics study section above.

The nonlinear Langmuir [48] equation has the following form:

$$q_e = q_m \frac{K_L C_e}{1+K_L C_e} \tag{7}$$

where q_m is the monolayer adsorption capacity (mg/g of adsorbent) and K_L is the Langmuir constant related to the energy of adsorption (L/mg). An important characteristic of Langmuir isotherm is the separation factor R_L, a dimensionless quantity calculated using the following equation:

$$R_L = \frac{1}{1+K_L C_i} \tag{8}$$

where C_i is the initial concentration of fluoride. For a favorable isotherm, the value of R_L should be between 0 and 1. The $R_L > 1$ and $R_L = 1$ suggest an unfavourable and a linear isotherm, respectively [42].

The Freundlich [49] equation is given as:

$$q_e = K_F C_e^{1/n} \tag{9}$$

where K_F is a Freundlich constant which indicates the sorption capacity of the adsorbent (mg/g adsorbent) $(L/mg)^{1/n}$, $1/n$ is a constant which gives the intensity of adsorption. For favorable adsorption, the value of K_F should be between 1 and 20 and the constant n must be above 1 [50]. The values of these constants are presented in Table 2. As the value of n in this study is above 1, as shown in Table 2, the adsorption is favorable.

The Temkin isotherm [51] equation is given as:

$$q_e = B_T \ln\left(K_T C_e\right) \tag{10}$$

where $B_T = RT/b$ is a constant related to the heat of adsorption, b is the variation of adsorption energy (J/mol), K_T is the Temkin constant which accounts for the interaction between the adsorbate and adsorbent (L/mg). The value of the constants is reported in Table 2.

The R^2 and SSE values reported in Table 2 indicate that the isotherm data is fairly represented by the Freundlich model at lower temperatures and by the Langmuir model at a higher temperature. An easy calculation of R_L, using Eq. (8) above, showed that R_L ranged between 0.43 to 0.13, for the concentrations 10, 20, 30, 40 and 50 mg/L, for all the temperatures considered here. This suggests a favorable adsorption isotherm. It is clear from Fig. 7 that the maximum uptake capacity appears to be significantly less than that predicted by the Langmuir model. Therefore, in the present work Langmuir isotherm could not be considered as a representative of the experimental isotherm data, although the R^2 values show reasonably good fitness.

3.9. Thermodynamics study

The thermodynamic parameters, namely, the standard Gibbs energy change (ΔG°), enthalpy change (ΔH°), and entropy change (ΔS°) of the adsorption of fluoride ions over BAC were determined by using the Eqs. (11) and (12) and the values for these parameters are presented in Table 3.

$$\Delta G^\circ = -RT \ln K_d \tag{11}$$

$$\Delta G^\circ = -RT \ln K_d = \Delta H^\circ - T\Delta S^\circ \tag{12}$$

$$\ln K_d = -\frac{\Delta H^\circ}{RT} + \frac{\Delta S^\circ}{R} \tag{13}$$

where T = temperature (K), R = universal gas constant (8.314 J/mol K), K_d = distribution coefficient, a function of temperature, calculated as, q_e/C_e. The value of ΔH° and ΔS°, reported in Table 3, were calculated from the slope and intercept of the plot between $\ln K_d$ vs. $1/T$, shown in Fig. 8.

The positive values of ΔG° in Table 3, suggest that adsorption was not spontaneous. Also, the increase in the

Table 3
Thermodynamic parameters for adsorption of fluoride on BAC

ΔG° (kJ/mol)				ΔH° (kJ/mol)	ΔS° (kJ/mol K)
16°C	26°C	36°C	46°C		
0.158	0.457	1.830	2.891	–30.30	–0.104

Table 1
Kinetic parameters for F^- removal by BAC (pH = 4.0; T = 289 K; BAC = 5.0 g/L; adsorbent size = 0.225 mm; F_i = 50 mg/L)

Temperature (°C)	Pseudo-first-order			Pseudo-second-order			Elovich model				Pore diffusion model		
	K_1	R^2	SSE	K_2	R^2	SSE	a	b	R^2	SSE	K_i	R^2	SSE
16	0.909	0.997	0.169	0.239	0.921	3.821	12.610	0.341	0.998	0.189	4.276	0.982	1.110
26	0.772	0.994	0.297	0.196	0.901	4.411	8.291	0.286	0.999	0.076	4.203	0.992	0.444
36	0.734	0.988	0.481	0.206	0.865	4.664	5.811	0.277	0.994	0.274	3.624	0.980	0.883
46	0.667	0.979	0.612	0.211	0.843	3.957	3.952	0.266	0.996	0.134	3.018	0.972	0.847

Table 2
Isotherm parameters for adsorption of F^- on BAC

Temperature (°C)	Langmuir				Freundlich				Temkin			
	q_m (mg/g)	K_L (L/mg)	R^2	SSE	n	K_F (mg/g)/(L/mg)$^{1/n}$	R^2	SSE	B_T (J/mol)	K_T (L/mg)	R^2	SSE
16	16.02	0.118	0.979	0.643	1.54	2.062	0.992	0.220	2.48	2.391	0.919	2.184
26	14.19	0.133	0.983	0.476	1.65	2.059	0.989	0.290	2.49	2.131	0.940	1.534
36	11.23	0.117	0.992	0.168	1.78	1.608	0.971	0.532	2.40	1.232	0.981	0.363
46	9.66	0.102	0.904	1.267	1.89	1.372	0.831	2.350	2.46	0.738	0.937	0.971

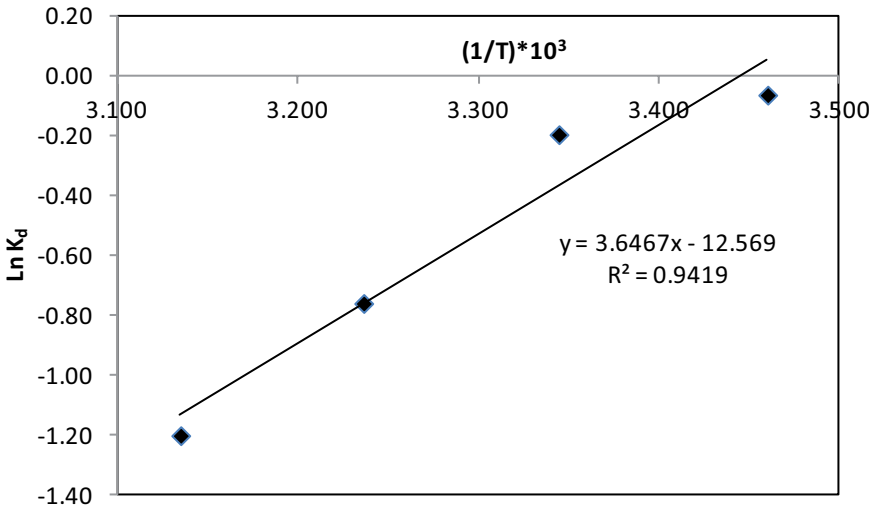

Fig. 8. Effect of temperature over distribution coefficient (K_d) for fluoride concentration of 50 mg/L, pH = 4 and adsorbent dose = 5 g/L.

Table 4
Comparison of BAC with other bisorbent studies on fluoride removal

Adsorbent	Initial fluoride concentration (mg/L)	Maximum adsorption capacity (mg/g)	Contact time (h)	Adsorbent dose (g/L)	% fluoride removal	Reference
Sugarcane bagasse	8	4.12	1	1	26	[19]
Activated KOH treated jamun seed	10	3.65	2	0.4	50	[17]
Activated carbon from barks of *Ficus racemosa*	5	1.65	1	4	88	[34]
Bael (*Aegle marmelos*) shell-activated	8	2.4	1	2	46	[16]
Tea waste-Al–Fe	10	18.52	2	2	90	[55]
$KMnO_4$ modified activated carbon of rice straw	5	15.9	3	1.5	70	[56]
Wheat straw raw	5	1.9	2	4.0	40.2	[18]
Activated bagasse carbon	5	1.15	2	4.0	56.4	[18]
Biochar from waste peanut shell powder	10	3.67	2	8	88.21	[57]
Zr loaded grape pomace	20	7.54	1	6	92	[58]
Citrus limetta residue	–	12.6	–	–	80–86	[59]
Zirconium impregnated camellia seed biochar	70	11.04	3	1.6	–	[60]
Modified material developed from *Ficus benghalensis* leaf	2		5	5	86.5	[61]
Al embedded *Thuja occidentalis* leaves carbon	10	0.625	1.5	20	92	[62]
Activated carbon derived from iron infused *Pisum sativum* peel	5	4.717	7	4	99	[63]
Artemia eggshell-zirconium nanocomposite	10	4.95	0.5	8	93	[64]
Tamarindus indica activated seed coat	5	1.79	1	0.3	92	[65]
Bagasse activated carbon	50	8.24 (16°C)	4	5	82.4	Present study
Bagasse activated carbon	50	8.04 (26°C)	4	5	80.4	Present study

positive value of $\Delta G°$ with the increase in temperature indicates that adsorption of F^- over BAC is less favorable at higher temperatures [17]. This adsorption trend was also confirmed by observing the values of K_d (Fig. 7) that decreased with the increase in temperature, indicating less distribution of sorbate between solid and solution phases. The plot between $\ln(K_d)$ and $1/T$, (K^{-1}) was fitted with a linear equation (R^2 = 0.9419) giving slope ($-\Delta H°/R$) and intercept ($\Delta S°/R$) as 3,646.7 and –12.57. The estimated value of enthalpy $\Delta H°$ and entropy $\Delta S°$ are reported in

Table 3. The negative value of $\Delta H°$ suggests the exothermic nature of the adsorption process [19]. According to the ranges of energy of adsorption for different forces; van der Waal forces 4–10 kJ/mol, hydrophobic bond forces about 5 kJ/mol, hydrogen bond forces 2–40 kJ/mol, coordination exchange about 40 kJ/mol, dipole bond forces 2–29 kJ/mol, chemical bond forces >60 kJ/mol, thus, it can be inferred that in the present adsorption process all the mechanisms except coordination exchange and chemical bond forces are possible [46,47,52,53]. However, the value obtained for $\Delta H°$ (–30.30 kJ/mol) suggests the dominance of physisorption over chemisorption [48,54]. The negative entropy $\Delta S°$ value shows that randomness in the aqueous phase was more compared to the solid phase [25].

3.10. Regeneration and reuse of BAC

The activated carbon was filtered and dried at 110°C for 6 h and again used for adsorption of F^-. For 10, 20 30, 40 and 50 mg/L F^- concentration in the solution, at pH 4, 26°C and 5 g/L of adsorbent dose. The final value of F^- concentration in the solution were 0.95, 3.1, 5.9, 7.9 and 11.1 mg/L. Whereas, the value of final F^- for fresh bagasse activated carbon was 0.8, 2.5, 4.7, 6.8 and 9.8 mg/L for the same condition of the adsorption process. Thus, a 14% to 25% decrease in adsorption efficiency was observed.

3.11. Performance of BAC compared to other biomass-based adsorbents for fluoride removal

A comparison of the performance of BAC with other biomass-derived adsorbents is presented in Table 4. A fair comparison is difficult due to a variety of process conditions, however, while comparing the performance of adsorbents the, initial concentration, adsorbent dose and contact time must be given sufficient weightage. A good adsorbent is expected to give significant fluoride removal within a reasonable contact time. Table 4 indicates that the contact time of 4 h in the present study is higher compared to other reported results but this may be attributed to the higher concentration of fluoride considered in the present work. The maximum adsorption capacity of BAC in this work, that is, 8.24 mg/g at 16°C, appears to be quite competitive with the capacity of the other adsorbents as reported in Table 4 reported. It also shows that the maximum adsorption capacity of the BAC in the present study is comparable to the other biosorbents.

4. Conclusion

Activated carbon was prepared from sugarcane bagasse to remove fluoride from synthetic fluoride-containing water. The study revealed that for an initial fluoride concentration of 10 mg/L, the final fluoride concentration can be reduced to 0.7 mg/L, that is, adsorption capacity equal to 1.86 mg/g, (within the limit prescribed by WHO) for initial pH value 4, adsorbent dose of 5 mg/L, temperature 16°C with 4 h of contact time, while that for 20 mg/L initial fluoride concentration it could be reduced to less than 4 mg/L final concentration (fluoride concentration limit set by USEPA) for 16°C, 26°C and 36°C temperatures, that is, adsorption capacity equal to 3.21 mg/g. The highest adsorption capacity was observed as 8.24 mg/g for 50 mg/L initial fluoride concentration at 16°C. The kinetic data fitted well with pseudo-first-order, pseudo-second-order, Elovich model and IPD models. The isothermal study showed a monolayer and multilayer adsorption mechanisms based on estimated coefficients and fitness of Langmuir, Freundlich and Temkin models. From the Langmuir model, it was observed that the maximum adsorption capacity of BAC was about 8–12 mg/g for a temperature range of 16°C–46°C, which appears very promising to make use of BAC in fluoride removal. Thermodynamic analysis showed that the present adsorption process was not spontaneous and exothermic as the value of $\Delta G°$ and $\Delta H°$ were positive and negative respectively. It can be concluded that BAC could be used as an inexpensive and benign adsorbent for the removal of fluoride from water.

References

[1] F. Shen, X. Chen, P. Gao, G. Chen, Electrochemical removal of fluoride ions from industrial wastewater, Chem. Eng. Sci., 58 (2003) 987–993.

[2] K. Chaudhary, P.K. Saraswat, S. Khan, Improvement in fluoride remediation technology using GIS based mapping of fluoride contaminated groundwater and microbe assisted phytoremediation, Ecotoxicol. Environ. Saf., 168 (2019) 164–176.

[3] L.S. Thakur, P. Mondal, Simultaneous arsenic and fluoride removal from synthetic and real groundwater by electrocoagulation process: parametric and cost evaluation, J. Environ. Manage., 190 (2017) 102–112.

[4] Meenakshi, R.C. Maheshwari, Fluoride in drinking water and its removal, J. Hazard. Mater., 137 (2006) 456–463.

[5] K.L. Saxena, R. Sewak, Fluoride consumption in endemic villages of India and its remedial measures, Int. J. Eng. Sci. Invention, 4 (2015) 2319–6734.

[6] K.K. Yadav, S. Kumar, Q.B. Pham, N. Gupta, S. Rezania, H. Kamyab, S. Yadav, J. Vymazal, V. Kumar, D.Q. Tri, A. Talaiekhozani, S. Prasad, L.M. Reece, N. Singh, P.K. Maurya, J. Cho, Fluoride contamination, health problems and remediation methods in Asian groundwater: a comprehensive review, Ecotoxicol. Environ. Saf., 182 (2019) 109362, doi: 10.1016/j.ecoenv.2019.06.045.

[7] K.L. Saxena, R. Sewak, R. Stea, Fluoride in groundwater: evaluation of removal methods, Int. J. Dev. Res., 6 (2016) 8339–8350.

[8] Y. Wang, N. Lin, Y. Gong, R. Wang, X. Zhang, Cu-Fe embedded cross-linked 3D hydrogel for enhanced reductive removal of Cr(VI): characterization, performance, and mechanisms, Chemosphere, 280 (2021) 130663, doi: 10.1016/j.chemosphere.2021.130663.

[9] Y. Wang, R. Wang, N. Lin, Y. Wang, X. Zhang, Highly efficient microwave-assisted Fenton degradation bishenol A using iron oxide modified double perovsike intercalated montmorillonite composite nanomaterial as catalyst, J. Colloid Interface Sci., 594 (2021) 446–459.

[10] Y. Wang, L. Yu, R. Wang, Y. Wang X. Zhang, Reactivity of carbon spheres template Ce/$LaCo_{0.5}Cu_{0.5}O_3$ in the microwave induced H_2O_2 catalytic degradation of salicylic acid: characterization, kinetic and mechanism studies, J. Colloid Interface Sci., 574 (2020) 74–86.

[11] Y. Yang, W. Ji, X. Li, Z. Zheng, F. Bi, M. Yang, J. Xu, X. Zhang, Insights into the degradation mechanism of perfluorooctanoic acid under visible-light irradiation through fabricating flower-shaped Bi_5O_7I/ZnO n-n heterojunction microspheres, Chem. Eng. J., 420 (2021) 129934, doi: 10.1016/j.cej.2021.129934.

[12] Y. Yang, Z. Zheng, M. Yang, J. Chen, C. Li, C. Zhang, X. Zhang, In-situ fabrication of a spherical-shaped Zn-Al hydrotalcite with BiOCl and study on its enhanced photocatalytic mechanism

for perfluorooctanoic acid removal performed with a response surface methodology, J. Hazard. Mater., 399 (2020) 123070, doi: 10.1016/j.jhazmat.2020.123070.
[13] L. Panda, B.B. Kar, Preparation of fly ash based zeolite for fluoride removal, Asian J. Water Environ. Pollut., 15 (2018) 105–113.
[14] R.M. Hegde, R.M. Rego, K.M. Potla, M.D. Kurkuri, M. Kigga, Bio-inspired materials for defluoridation of water: a review, Chemosphere, 253 (2020) 126657, doi: 10.1016/j.chemosphere.2020.126657.
[15] S. Mukherjee, G. Halder, A review on the sorptive elimination of fluoride from contaminated wastewater, J. Environ. Chem. Eng., 6 (2018) 1257–1270.
[16] K. Singh, D.H. Lataye, K.L. Wasewar, Removal of fluoride from aqueous solution by using Bael (*Aegle marmelos*) shell activated carbon: kinetic, equilibrium and thermodynamic study, J. Fluorine Chem., 194 (2017) 23–32.
[17] R. Araga, S. Soni, C.S. Sharma, Fluoride adsorption from aqueous solution using activated carbon obtained from KOH-treated jamun (*Syzygium cumini*) seed, J. Environ. Chem. Eng., 5 (2017) 5608–5616.
[18] A.K. Yadav, R. Abbassi, A. Gupta, M. Dadashzadeh, Removal of fluoride from aqueous solution and groundwater by wheat straw, sawdust and activated bagasse carbon of sugarcane, Ecol. Eng., 52 (2013) 211–218.
[19] K. Singh, D.H. Lataye, K.L. Wasewar, Removal of fluoride from aqueous solution by using low-cost sugarcane bagasse: kinetic study and equilibrium isotherm analyses, J. Hazard. Toxic Radioact. Waste, 20 (2016) 1–13.
[20] J.X. Sun, R.C. Sun, X.F. Sun, Y.Q. Su, Fractional and physico-chemical characterization of hemicelluloses from ultrasonic irradiated sugarcane bagasse, Carbohydr. Res., 339 (2004) 291–300.
[21] Global Agriculture Information Network (GAIN), Report Number IN8047.
[22] Y.S. Antaresti, H.W. Setiyadi, Y.P. Yogi, The Effect of Chemical and Biopulping Process to Bagasse Pulp, Proceeding of RSCE and SOMChe, Petaling Jaya, Malaysia, 2002, pp. 639–644.
[23] X. Zhang, F. Bi, Z. Zhu, Y. Yang, S. Zhao, J. Chen, X. Lv, Y. Wang, J Xu, N. Liu, The promoting effect of H_2O on rod-like MnCeOx derived from MOFs for toluene oxidation: a combined experimental and theoretical investigation, Appl. Catal., B, 297 (2021) 120393, doi: 10.1016/j.apcatb.2021.120393.
[24] X. Zhabg, Y. Yang, Q. Zhu, M. Ma, Z. Jiang, X. Liao, C. He, Unraveling the effects of potassium incorporation routes and positions on toluene oxidation over α-MnO_2 nanorods: based on experimental and density functional theory (DFT) studies, J. Colloid Interface Sci., 598 (2021) 324–338.
[25] N. Azouaou, Z. Sadaoui, A. Djaafri, H. Mokaddem, Adsorption of cadmium from aqueous solution onto untreated coffee grounds: equilibrium, kinetics and thermodynamics, J. Hazard. Mater., 184 (2010) 126–134.
[26] I. Tüzün, G. Bayramoğlu, E. Yalçin, G. Başaran, G. Çelik, M.Y. Arica, Equilibrium and kinetic studies on biosorption of Hg(II), Cd(II) and Pb(II) ions onto microalgae *Chlamydomonas reinhardtii*, J. Environ. Manage., 77 (2005) 85–92.
[27] S. Chidambaram, A.L. Ramanathan, S. Vasudevan, Fluoride removal studies in water using natural materials, Water SA, 29 (2003) 339–343.
[28] Y. Tang, X. Guan, J. Wang, N. Gao, M.R. McPhail, C.C. Chusuei, Fluoride adsorption onto granular ferric hydroxide: effects of ionic strength, pH, surface loading, and major co-existing anions, J. Hazard. Mater., 171 (2009) 774–779.
[29] R. Bhaumik, N.K. Mondal, S. Chattoraj, An optimization study for defluoridation from synthetic fluoride solution using scale of Indian major carp Catla (*Catla catla*): an unconventional biosorbent, J. Fluorine Chem., 195 (2017) 57–69.
[30] P.S. Ghosal, A.K. Gupta, An insight into thermodynamics of adsorptive removal of fluoride by calcined Ca-Al-(NO_3) layered double hydroxide, RSC Adv., 5 (2015) 105889–105900.
[31] D. Mehta, P. Mondal, S. George, Utilization of marble waste powder as a novel adsorbent for removal of fluoride ions from aqueous solution, J. Environ. Chem. Eng., 4 (2016) 932–942.
[32] S. Chakrabarty, H.P. Sarma, Defluoridation of contaminated drinking water using neem charcoal adsorbent: kinetics and equilibrium studies, Int. J. ChemTech Res., 4 (2012) 511–516.
[33] S.V. Mohan, J. Karthikeyan, Removal of lignin and tannin colour from aqueous solution by adsorption onto activated charcoal, Environ. Pollut., 97 (1997) 183–187.
[34] S. Ravulapalli, K. Ravindhranath, Defluoridation studies using active carbon derived from the barks of *Ficus racemosa* plant, J. Fluorine Chem., 193 (2017) 58–66.
[35] S. Lagergren, Zur theorie der sogenannten adsorption geloster stoffe, Kungliga Svenska Vetenskapsakademiens. Handligar, J. Sci. Res., 24 (1898) 1–39.
[36] Y.S. Ho, G. Mckay, T. Hong, W. Bay, H. Kong, T. Hong, Kinetics of pollutant sorption by biosorbents: review, Sep. Purif. Rev., 2 (2011) 189–232.
[37] S.H. Chien, W.R. Clayton, Application of Elovich equation to the kinetics of phosphate release and sorption in soils, Soil Sci. Soc. Am. J., 44 (1980) 265–268.
[38] W.J. Weber, J. Carrell Morris, Kinetics of adsorption on carbon from solution, J. Sanit. Eng. Div., 89 (1963) 31–60.
[39] K.V. Kumar, K. Porkodi, F. Rocha, Comparison of various error functions in predicting the optimum isotherm by linear and non-linear regression analysis for the sorption of Basic red 9 by activated carbon, J. Hazard. Mater., 150 (2008) 158–65.
[40] J. Lin, L. Wang, Comparison between linear and non-linear forms of pseudo-first-order and pseudo-second-order adsorption kinetic models for the removal of methylene blue by activated carbon, Front. Environ. Sci. Eng. China, 3 (2009) 320–324.
[41] Markandeya, S.P. Shukla, G.C. Kisku, Linear and non-linear kinetic modeling for adsorption of disperse dye in batch process, Res. J. Environ. Toxicol., 9 (2015) 320–331.
[42] F. Togue Kamga, Modeling adsorption mechanism of paraquat onto Ayous (*Triplochiton scleroxylon*) wood sawdust, Appl. Water Sci., 9 (2019) 1–7.
[43] C.S. Ngakou, G.S. Anagho, H.M. Ngomo, Non-linear regression analysis for the adsorption kinetics and equilibrium isotherm of phenacetin onto activated carbons current, J. Appl. Res. Technol., 36 (2019) 1–18.
[44] K.L. Tan, B.H. Hameed, Insight into the adsorption kinetics models for the removal of contaminants from aqueous solutions, J. Taiwan Inst. Chem. Eng., 74 (2017) 25–48.
[45] V. Sivasankar, S. Rajkumar, S. Murugesh, A. Darchen, Influence of shaking or stirring dynamic methods in the defluoridation behavior of activated tamarind fruit shell carbon, Chem. Eng. J., 197 (2012) 162–172.
[46] B. Acevedo, C. Barriocanal, I. Lupul, G. Gryglewicz, Properties and performance of mesoporous activated carbons from scrap tyres, bituminous wastes and coal, Fuel, 151 (2015) 83–90.
[47] S. Meshram, C. Thakur, A.B. Soni, Adsorption of Pb(II) form battery recycling unit effluent using granular activated carbon (GAC) and steam activated GAC, Indian Chem. Eng., (2020) 1–18, doi: 10.1080/00194506.2020.1795933.
[48] Langmuir, The adsorption of gases on plane surfaces of glass, mica and platinum, J. Am. Chem. Soc., 40 (1918) 1361–1368.
[49] H.M.F. Freundlich, Over the adsorption in solution, J. Phys. Chem., 57 (1906) 385–471.
[50] F. Batool, J. Akbar, S. Iqbal, S. Noreen, S.N.A. Bukhari, Study of isothermal, kinetic, and thermodynamic parameters for adsorption of cadmium: an overview of linear and nonlinear approach and error analysis, Bioinorg. Chem. Appl., 2018 (2018) 1–11.
[51] M.J. Temkin, V. Pyzhev, Recent modifications to Langmuir isotherms, Acta Physiochim. U.S.S.R, Adv. Chem. Eng., 12 (1940) 217–222.
[52] Y. Ma, N. Gao, W. Chu, C. Li, Removal of phenol by powdered activated carbon adsorption, Front. Environ. Sci. Eng., 7 (2013) 158–165.
[53] B. von Oepen, W. Kördel, W. Klein, Sorption of nonpolar and polar compounds to soils: processes, measurements and experience with the applicability of the modified OECD-Guideline 106, Chemosphere, 22 (1991) 285–304.

[54] V. Gopal, K.P. Elango, Equilibrium, kinetic and thermodynamic studies of adsorption of fluoride onto plaster of Paris, J. Hazard. Mater., 141 (2007) 98–105.
[55] H.M. Cai, G.J. Chen, C.Y. Peng, Z.Z. Zhang, Y.Y. Dong, G.Z. Shang, X.H. Zhu, H.J. Gao, X.C. Wan, Removal of fluoride from drinking water using tea waste loaded with Al/Fe oxides: a novel, safe and efficient biosorbent, RSC Adv., 328 (2015) 34–44.
[56] A.A.M. Daifullah, S.M. Yakout, S.A. Elreefy, Adsorption of fluoride in aqueous solutions using $KMnO_4$-modified activated carbon derived from steam pyrolysis of rice straw, J. Hazard. Mater., 147 (2007) 633–643.
[57] P. Kumar, A.K. Prajapati, S. Dixit, V.L. Yadav, Adsorption of fluoride from aqueous solution using biochar prepared from waste peanut hull, Mater. Res. Express, 6 (2020) 125553.
[58] Y. Zhang, K. Huang, Grape pomace as a biosorbent for fluoride removal from groundwater, R. Soc. Chem., 9 (2019) 7767–7777.
[59] M. Ibrahim, A. Siddique, L. Verma, J. Singh, J.R. Koduru, Adsorptive removal of fluoride from aqueous solution by biogenic iron permeated activated carbon derived from sweet lime waste, Acta Chim. Slov., 66 (2019) 123–136.
[60] L. Mei, H. Qiao, F. Ke, C. Peng, R. Hou, X. Wan, H. Cai, One-step synthesis of zirconium dioxide-biochar derived from *Camellia oleifera* seed shell with enhanced removal capacity for fluoride from water, Appl. Surf. Sci., 509 (2020) 144685, doi: 10.1016/j.apsusc.2019.144685.
[61] N.G. Telkapalliwar, Defluoridation of water by using modified material deceloped from *Ficus benghalensis* leaf: characterization, kinetic and thermodynamic study, IOP Conf. Ser.: Mater. Sci. Eng., 983 (2020) 012008.
[62] D.R. Vaddhi, V.S.R. Mushini, P.S.M. Mudumba, Use of aluminium metal embedded *Thuja occidentalis* leaves carbon (AMETLC) for fluoride removal from water: equilibrium and kinetic studies, J. Environ. Treat., 9 (2021) 480–490.
[63] N. Sahu, C. Bhan, J. Singh, Removal of fluoride from an aqueous solution by batch and column process using activated carbon derived from iron infused *Pisum sativum* peel: characterization, isotherm, kinetics study, Environ. Eng. Res., 26 (2021) 200241.
[64] W. Zhang, Y. Mao, Y. Lu, Development of a novel Artemia eggshell-zirconium nanocomposite for efficient fluoride removal, PLoS One, 16 (2021) e0244711.
[65] D. Srinivasulu, P.K. Pindi, Activated tamarind seed coat: a green biosorbent to remove fluoride from aqueous solutions, Water Supply, 21 (2021) 1594–1607.